



Effect of stress amplitude on mechanical and acoustic emission of sandstone under constant–cyclic loading

Bichuan Zhang^{1,2} · Yunpei Liang^{1,2} · Zhanyi Zhao³ · Quanle Zou^{1,2} · Haolong Zheng^{1,2} · Yanhao Ning^{1,2} · Fanjie Kong^{1,2} · Qican Ran^{1,2}

Received: 13 September 2022 / Accepted: 11 May 2023 / Published online: 30 June 2023
© Springer-Verlag GmbH Germany, part of Springer Nature 2023

Abstract

The mechanical characteristics of sandstone under constant–cyclic loading with different amplitudes play a significant role in geotechnical engineering. In this research, constant–cyclic tests with stress amplitudes of 5%, 10%, and 15% of the uniaxial compressive strength were conducted to analyse the effect of stress amplitude on the mechanical behaviours of sandstone. Then, the internal crack propagation of sandstone was characterized based on the real-time record of an acoustic emission (AE) technique. Finally, the fragments of the rock mass distribution and failure pattern were assessed. The results showed that the cyclic deformation, acoustic emission response, fragmentation characteristics, and internal cracks depend strongly on the stress amplitude. With increasing stress amplitude, the peak strength first increases and then decreases. There may exist a specific loading amplitude that increases the peak strength. In addition, a higher stress amplitude may lead to peak strength degradation to some extent. In addition, the elastic and dissipated energy shows decreasing and increasing trends in the cyclic loading stages, respectively. Elastic energy accounts for the largest proportion of all input energy. The fragment distribution is more uneven, the percentage of large and small blocks increases, and the failure patterns are more complex under higher stress amplitudes, which can reveal the fracture characteristics of the sandstone under different amplitudes. These results can offer a reference to understand the different disruption effects on the engineering characteristics of sandstone and play a guiding role in the mining-induced stress boundary movement and control of dynamic disasters.

Keywords Sandstone · Stress amplitude · Constant–cyclic loading · Acoustic emission · X-ray CT · Energy evolution

Introduction

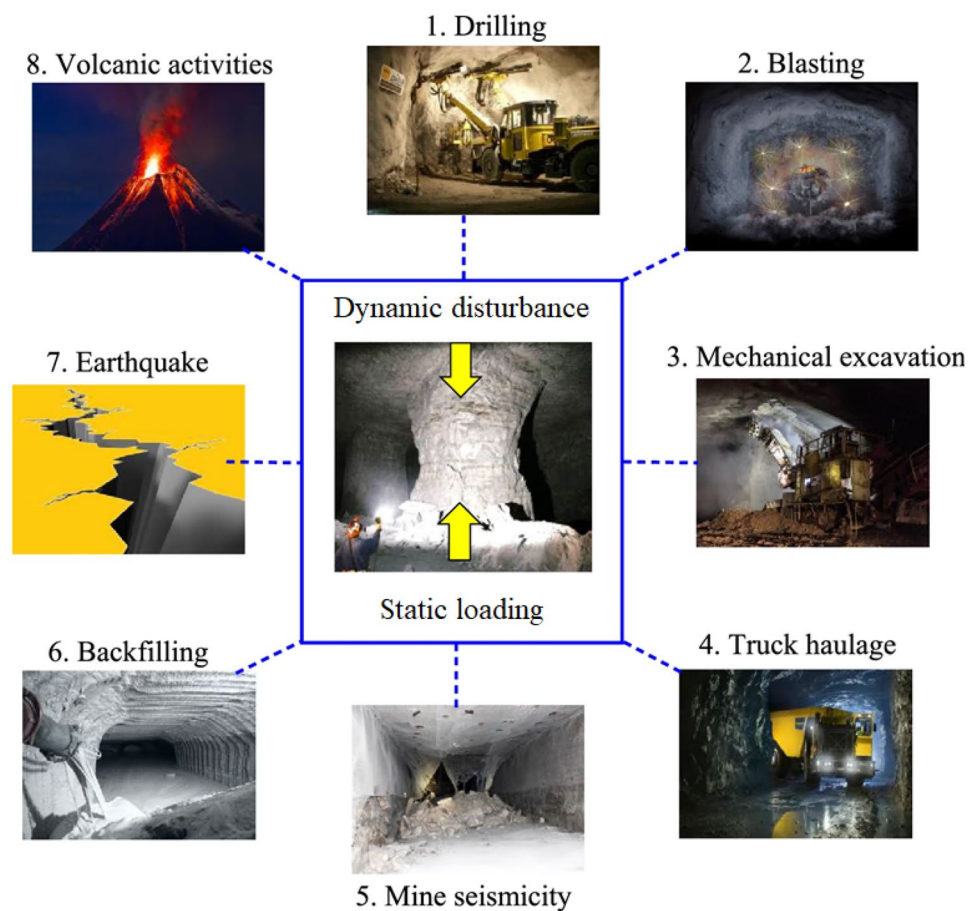
Sandstone is one of the most common research objects in various geotechnical engineering applications, such as coal mining (Zhang et al. 2020; Xia et al. 2021; Liang et al. 2022), mining-induced boundary movement (Sun et al. 2019), landslide control (Yang et al. 2020a, b), energy storage (Wang et al. 2011; Zhao et al. 2021; Zou et al. 2022a, b), and other human-made structures (Yang et al. 2020a,

b; Zhang et al. 2021). Sandstone in different positions of geotechnical engineering, such as mining-induced boundary movement, will experience various disturbance types. These applications highlight the urgent need to better understand the behaviours of rock-related structures under environmental and human-induced disturbances (Zhu et al. 2019; Du et al. 2020) (Fig. 1). Environmental and human-induced disturbances are essentially cyclic and constant under laboratory conditions (Cerfontaine and Collin 2018; Zou et al. 2022a, b). Thus, the mechanical characteristics of specific rocks have drawn much attention from many scholars, and these are crucial in designing and building structures (Zhao et al. 2017, 2021; Yang and Hu 2018; Young et al. 2020). Previous studies found that rock deformation and damage characteristics under different cyclic loading and unloading significantly differ from those under a single monotonic loading path (Fuenkajorn and Phueakphum 2010; Ran et al. 2023). Stress amplitude, loading frequency, and waveform are the main cyclic loading parameters that affect the

✉ Yunpei Liang
liangyunpei@126.com

¹ State Key Laboratory of Coal Mine Disaster Dynamics and Control, Chongqing University, Chongqing 400044, China
² School of Resources and Safety Engineering, Chongqing University, Chongqing 400044, China
³ Ningxia Vocational College of Sports, Ningxia 750021, China

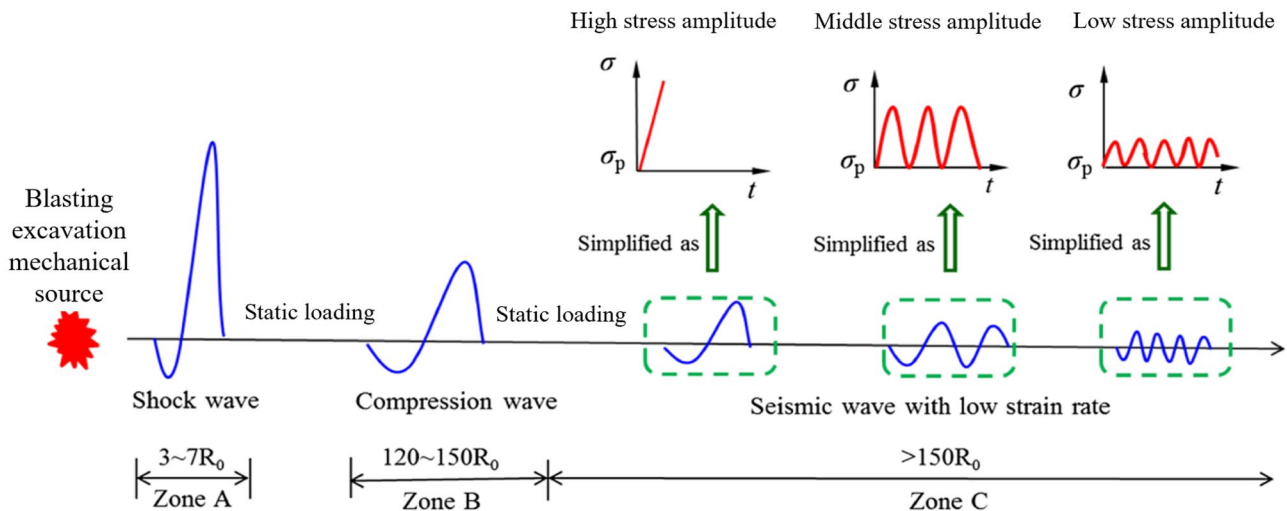
Fig. 1 Different sources of disturbances imposed on underground structures (Shirani Faradonbeh et al. 2021)



mechanical behaviours of sandstone (Cerfontaine and Collin 2018; Liu et al. 2018; Vaneghi et al. 2018; Zhu et al. 2020).

Blasting (Khandelwal and Singh 2009; Konicek et al. 2013), excavation (Demirel 2011), and mechanical vibration (Zhang et al. 2016) are the main sources that generate disturbances in practical engineering. With increasing distance from disturbance sources, the shock wave will evolve from higher stress or seismic amplitude to lower amplitude (Fig. 2). Similar to the three constant stages, the rock damage under cyclic loading can also be divided into an initial loading stage, a uniform stage, and an accelerated deformation stage (Zhu et al. 2020). The stress amplitude level is a significant factor affecting the damage properties of rocks (Momeni et al. 2015; Vaneghi et al. 2020). The greater the loading cycle number is, the shorter the rock lifetime and the greater the strength degradation (Vaneghi et al. 2018). The effect of the stress amplitude on the dynamic elastic modulus was more significant than that on the damping coefficient (Deng et al. 2017). Rocks will harden under lower stress amplitudes and soften under higher stress amplitudes (Shi et al. 2014). The critical normalized stress amplitude depends on the rock type and composition (Taheri et al. 2016; Li et al. 2021). The rock lifetime decreases as the stress amplitude increases (Du et al. 2021).

Rock progressive failure is a process of external energy input, inter-energy accumulation, and excessive energy release (Hua and You 2001). The energy perspective can deepen the understanding of the mechanical behaviour of failed rocks and promote the understanding of disaster mechanisms (Meng et al. 2019; Ammirati et al. 2022). With the stress state and corresponding deformation changes under specific cyclic loading paths, the energy state and microcracks of rock will evolve, leading to microcrack propagation (Sang et al. 2020; Zhang and Zhou 2022). These macrocracks gather and form a fault plane and cause overall instability (Meng et al. 2019). The deformation process of rock specimens under single cyclic loading is an irreversible dissipation process, and failure is the final result containing a larger-scale energy release (Zhang et al. 2019). Energy release shows a positive correlation with frequency (Bagde and Petros 2009). Energy dissipation drives the crack propagation procedure (Duan and Yang 2018; Wang et al. 2020). Thus, the increase in energy dissipated under cyclic loading will lead to a gradual decrease in the dynamic elastic modulus (He et al. 2015). Many methods can determine crack propagation and rock failure (Cai et al. 2014; Munoz and Taheri 2017; Yang et al. 2018). As a reliable and widely used testing method, acoustic emission (AE) has attracted significant attention in investigating damage evolution, crack



σ_p is the initial static stress preceding dynamic disturbance loading
 R_0 is the charging of influence

Fig. 2 Blasting, excavation, mechanical wave attenuation, and seismic wave simplification in a long-term constant–cyclic procedure (Li et al. 2017; Luo et al. 2019)

development, and failure in real time (Lockner 1993; Ruck et al. 2017; Zhang et al. 2022). In addition, the AE method can determine the accurate crack position and describe the whole procedure that contains the initiation, propagation, and coalescence of new cracks (Meng et al. 2018; Dong et al. 2022; He et al. 2022). AE signals will be more noticeable when the loading stress exceeds the previous loading stress threshold (Kao et al. 2011; Sagar and Prasad 2012). In addition, the precursory time series of the rise time rate is also a good indicator to forecast the pseudo-prospective of catastrophic rupture (Zhang and Zhou 2020). Thus, this method will be more effective under multilevel cyclic loading stress (Lavrov 2001).

In general, microcracks exist in all kinds of rocks (Liu et al. 2017). Failure modes are impacted by interbeds, natural fractures, and pyrite bands (Wang et al. 2021). There are two ways to investigate the failure mode after an experiment. One is to take photos of specimens to analyse the failure mode through superficial failure characteristics (Liu et al. 2018; Xiao et al. 2020), and then the fragment distribution (Ning et al. 2019) and fractal dimension (Li et al. 2018a, b) can be obtained. However, it is challenging and unrealistic work to investigate the internal crack characteristics of rock specimens through surface observations (Wang et al. 2019). Thus, another method, CT scanning, has been introduced to study the internal damage of rock. Cyclic loading induces new cracks and the propagation of existing cracks (Akesson et al. 2004), and stress-induced trials are less smooth and bright than static loading (Erarslan 2016). The crack network pattern becomes complex as the stress amplitude increases (Wang et al. 2020).

The studies mentioned above were primarily conducted under single cyclic loading. However, sandstone in specific geotechnical engineering often experiences different amplitudes of cyclic and constant loading due to various disturbances in actual rock-related engineering, such as mining-induced boundary movement, blasting, and excavation. In addition, artificial structures in engineering will serve a specific long-term period that plays a vital role in rock degradation. The rock response under constant–cyclic loading is different from that under single cyclic loading. To reveal the comprehensive mechanical response of sandstone, a series of different stress amplitude constant–cyclic tests were conducted. The influence of stress amplitude on the progressive mechanical response staged acoustic emission and postfracture behaviour of sandstones in constant–cyclic tests was investigated in this paper. During the constant–cyclic loading process, real-time AE was used to analyse the crack propagation characteristics. Ultimately, the crack distribution of sandstone specimens is revealed by CT scanning. Through the cross-sections and reconstruction of sandstone specimens, the fracture mechanism of sandstone under various cyclic amplitudes is revealed.

Sample preparation and test procedure

The sandstone specimens in this experiment were obtained from Hunan Province in China. Twenty-five specimens were carefully prepared by cutting $\Phi 50 \text{ mm} \times 100 \text{ mm}$ cylindrical specimens according to the standard ISRM guidelines. In addition, to ensure the reliability of the

experimental results as much as possible, 3 specimens with similar P wave velocity and average density values were selected to guarantee the consistency of the specimens (Table 1). Before the constant–cyclic tests, three specimens were used to determine the average uniaxial compression strength (UCS), which was approximately 48 MPa. The mineral components of sandstone were measured by X-ray diffraction (XRD) and were mainly composed of dickite (41%) and quartz (37.2%).

Different amplitude multilevel constant–cyclic tests were conducted using a rock compression system. A flat cylinder striker can offer a cyclic triangle stress wave and a long-term stable mechanical environment and can be used to conduct different amplitude constant–cyclic tests, abbreviated as ACF. Two nano-30 type AE sensors were set at the symmetrical position of the samples. The threshold was set as 40 dB. Figure 3 shows the stress-loading path of the ACF tests, which consists of three constant–cyclic stages and different stress amplitudes. A stress mode at a speed of 400 N/s in the axial direction was applied to the sandstone during the cyclic and constant loading stages. In the cyclic procedure, the cyclic stress amplitude varies by approximately 5%, 10%, and 15% of UCS. The constant loading stress was 25 and 32 MPa in the first and second constant–cyclic loading stages, respectively, and all the hold times were 2 h. When the sandstone specimens failed, the ACF tests stopped. Ultimately, the X-ray CT scanning method was used to reveal the internal fracture characteristics of sandstone specimens. In addition, systematic sieving tests were conducted to quantify the influence of stress amplitude on the fragment characteristics of sandstone specimens. The detailed testing procedures are illustrated in Fig. 4.

Results

Mechanical characteristics of sandstone under the constant–cyclic test

The stress–strain curves of sandstone at different amplitude constant–cyclic tests are plotted in Fig. 5a–c. Sandstone specimen deformation under different amplitude constants

Table 1 P wave velocity and density distribution

No	P wave velocity (km/s)	Density (kg/m ³)	Length (mm)	Diameter (mm)
1#	3.00	2390	100.4	50.2
2#	3.04	2450	101.1	49.5
3#	3.01	2430	100.7	50.0

and cycles shows a noticeable difference under different stress amplitudes. In the first 5%, 10%, and 15% amplitude cyclic loadings, those specimens' strains were 0.03%, 0.06%, and 0.104%, respectively. The irreversible deformation of different samples showed a nonlinear increment of approximately 0.04%. The sandstone matrix elastic characteristics may dominate this cyclic stage. In the second 5%, 10%, and 15% amplitude cyclic loading stage, the specimen strains were 0.02%, 0.05%, and 0.083%, respectively. In the first stage, axial deformation proliferated due to fracture compression and elastic deformation. In the second stage, the axial deformation corresponded well with the increment of stress amplitude. Three specimens all failed at the third constant–cyclic stage. Figure 5 also shows the failure modes of sandstone specimens under constant–cyclic loading. The maximum stresses of the three sandstones were 39.2 MPa, 40.5 MPa, and 39.3 MPa at 5%, 10%, and 15% stress amplitudes, respectively. The sandstone specimens experienced some shear or tensile cracks, which show brittle failure characteristics of the sandstone under constant–cyclic loading. Furthermore, the specimens also displayed some differences, even though the three specimens show mainly shear fracture modes, which may result from the effect of the heterogeneity of sandstone. However, with increasing stress amplitude, the final failure form was more violent, and broken rock fragments were hard to join, which indicates that the integrity of the rock was reduced under higher stress amplitude.

AE characteristics and energy dissipation of sandstone

Elastic and dissipated energy evolution before the peak stress

The input, elastic, and dissipated energy in each cycle of different stress amplitudes can be obtained based on the stress–strain curves. It is assumed that there is no heat, light, or other forms of energy release. The external input energy U^t is equal to the sum of elastic and dissipated energy (Li et al. 2020):

$$U^t = U^e + U^d \quad (1)$$

where U^e is the elastic energy and U^d is the dissipated energy.

Figure 6 shows the relationship between the elastic energy and dissipated energy of rock. The area region below the stress–strain curve denotes the external input energy, and the part under the unloading curves represents elastic energy. The region under the loading curves and above the unloading curves is the dissipated energy, which indicates plastic deformation, internal damage, and other kinds of dissipated energy. The equation of related energy can be expressed as Eq. (2) (Zhou et al. 2019):

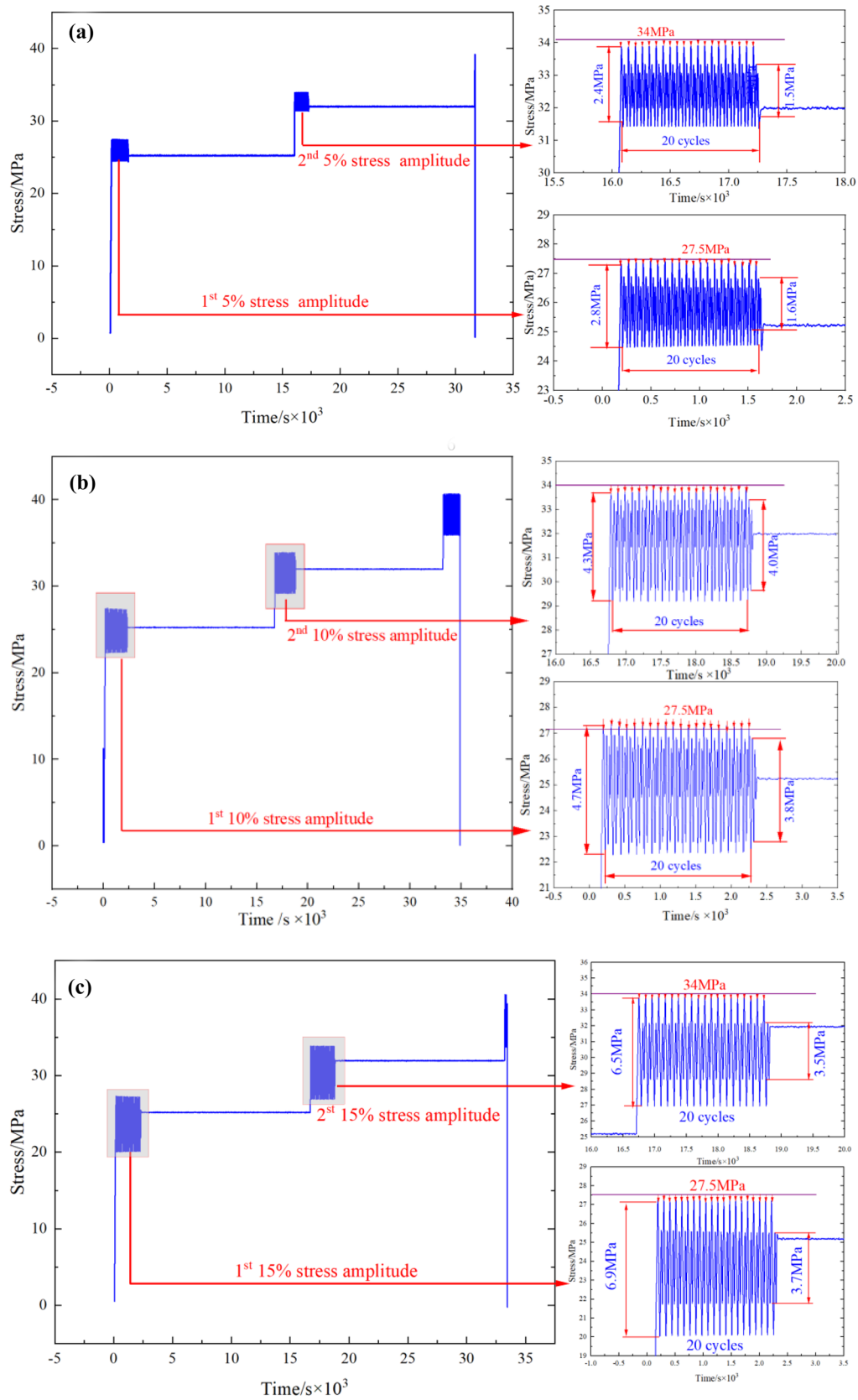


Fig. 3 Stress–time curves of multilevel ACF tests: **a** 5% stress amplitude, **b** 10% stress amplitude, and **c** 15% stress amplitude

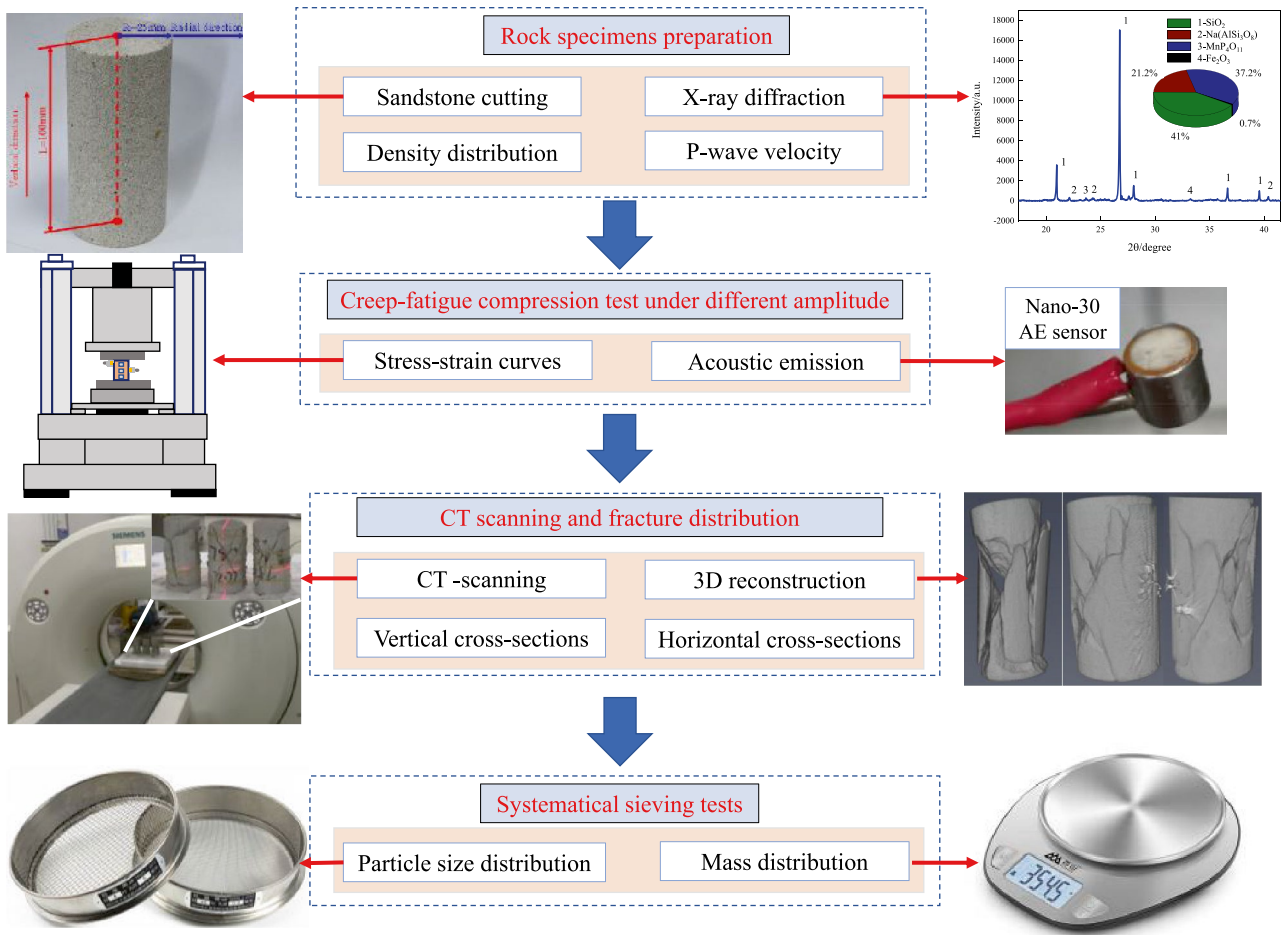


Fig. 4 Experimental procedures and equipment

$$\begin{cases}
 U = \int_0^{\epsilon''} \sigma_1 d\epsilon_1 \\
 U^e = \int_{\epsilon''}^{\epsilon'} \sigma_1 d\epsilon_1 \\
 U^d = U - U^e = \int_0^{\epsilon''} \sigma_1 d\epsilon_1 - \int_{\epsilon''}^{\epsilon'} \sigma_1 d\epsilon_1
 \end{cases} \quad (2)$$

The proportions of the elastic and dissipated energy distributions in the first and last cycles are shown in Fig. 7. Elastic energy is the leading energy in all cyclic loading amplitudes, at approximately 88% of the total energy. The proportion of elastic energy decreased at higher stress

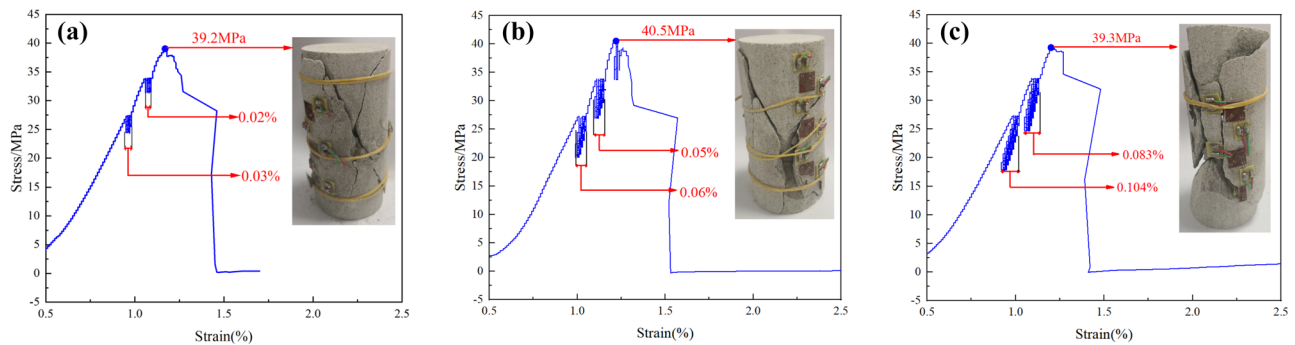


Fig. 5 Stress–strain curves of sandstone specimens at different amplitude constant–cyclic tests (a, b, and c represent 5%, 10%, and 15% cyclic stress amplitudes, respectively)

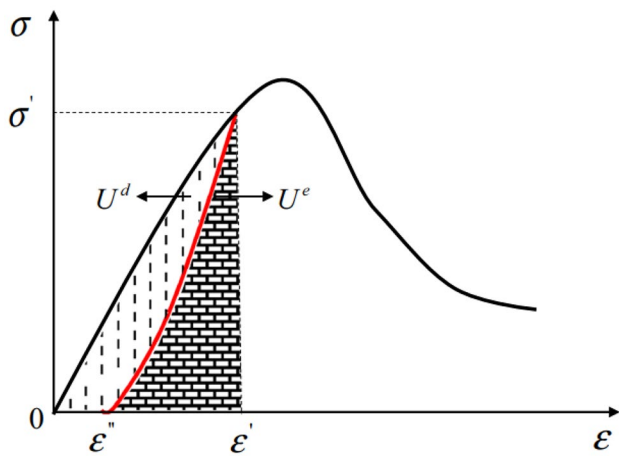


Fig. 6 Relationship between external input energy, elastic energy, and dissipated energy of sandstone in single cyclic loading (Zhou et al. 2019)

amplitudes. In addition, the proportion of elastic energy also decreased under different stress amplitudes in the same loading procedure. However, the proportion of dissipated energy rises at higher stress amplitudes. Therefore, as the external input energy increases, the dissipated energy will also increase correspondingly, which subsequently causes rock damage.

AE events during the constant-cyclic test

The RA value is the ratio of the rise time of the AE signal to its amplitude, and the combination of RA and AF can be used to describe the fracture mode classification of rock materials (Zhang et al. 2020; Rodriguez and Celestino 2019). A combination of lower RA values and higher AF values results from the tensile mode. In contrast, a higher RA value and lower AF value indicate a shear mode (Liu et al. 2020).

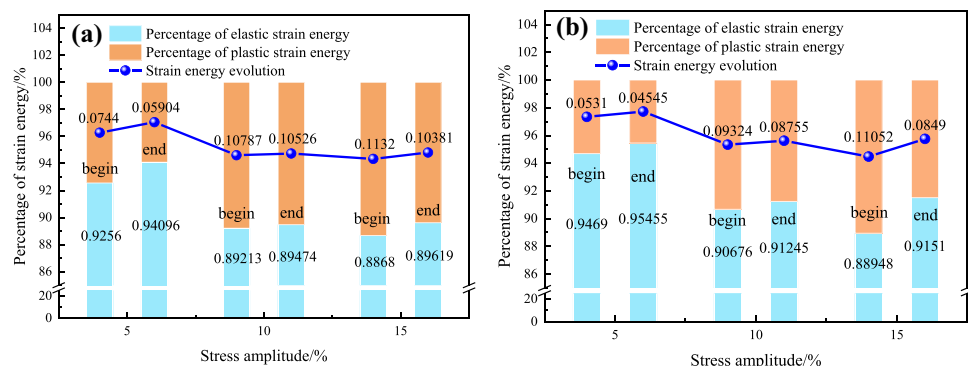
Figure 8 shows the typical RA and AF value variation with time in constant-cyclic stress at various amplitudes. The AF values of the sandstone specimens are mainly distributed in the range of 0~250 kHz, while the RA values

are mainly located in the range of 0~18 ms/V. With the increase in stress amplitude applied to the sandstone specimens, the RA and AF values increase in both stages (Fig. 8a and b). At the 1st stage, the increase in the RA value and the decrease in the AF value indicate the tensile mode. With the stress amplitude increasing from 5 to 10% and 15% UCS, the transition from lower RA and AF values to higher RA and AF values means a greater extent of tensile mode (Fig. 8a). This indicates that the tensile mode was the dominant failure form in the rock sample at different amplitudes in the initial loading stage. As the cyclic stress amplitude increased to a certain level, the RA and AF values increased approximately 100 times, which means that the shear mode was dominant in the sandstone in the second stage at different amplitudes.

RA-AF distribution can also be used for the qualitative classification of crack propagation form (Liu et al. 2020). As shown in Fig. 9, the RA-AF value with different amplitudes was mainly distributed at the first and second stages. In the first stage, with increasing stress amplitude, the failure mode transferred from almost equal tensile and shear to a tensile- or shear-dominated mode (Fig. 9a, b, and c). This kind of change will occur at higher stress levels. The shear or tensile crack propagation mode is almost equal at a lower stress amplitude. At higher stresses, the stress amplitude effect was similar, except for some lower cyclic amplitudes. This may occur because a lower amplitude may not significantly impact the failure mode.

Based on the analysis of failure modes considering the RA and AF values, when cyclic loading is applied at a lower stress level, crack evolution may be dominated by the tensile mode (Fig. 9b) or shear mode (Fig. 9c). However, when the stress level increased, the shear model dominated the crack evolution procedure (Fig. 9d, e, and f). When the load was close to the peak stress, the shear cracks increased, and the ultimate failure mode of the specimens mainly appeared as shear failure. These results are consistent with the analysis of the failure mode of sandstone specimens in the “Macro-failure characteristics of sandstone under a constant-cyclic test” section.

Fig. 7 Characteristics of the energy proportion under 5%, 10%, and 15% cyclic amplitude: **a** 1st stage and **b** 2nd stage



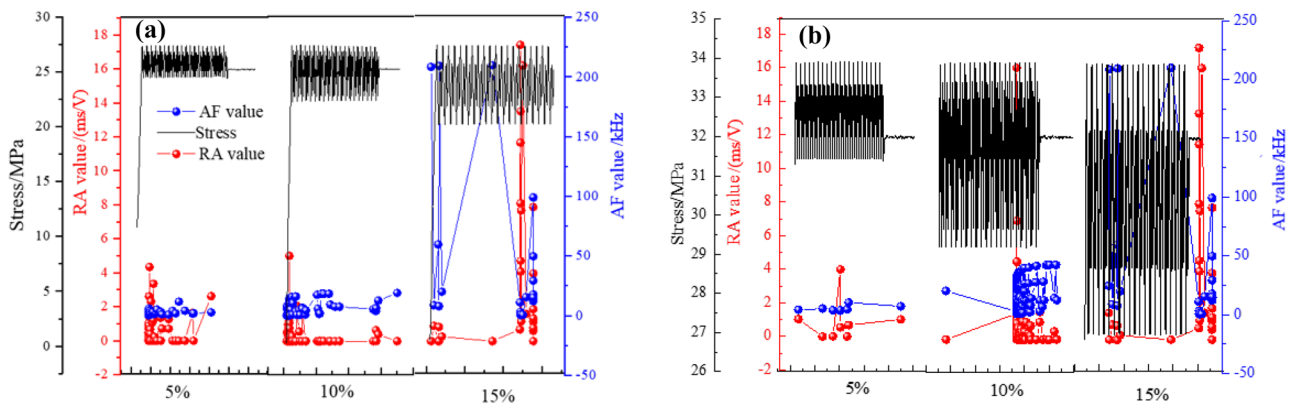


Fig. 8 Stress, RA, and AF value versus time at 5%, 10%, and 15% cyclic loading amplitude: **a** 1st stage and **b** 2nd stage

Peak frequency in cyclic loading is vital for characterizing the crack source properties (K 1962). Different types of disturbance sources will produce different scale fractures for specific rock specimens. Lower frequency signals represent larger-scale cracks. The distribution of the peak frequency of AE signals in different stages offers noticeable zone features, and these peak frequencies are in ranges of 0–15 kHz, 15–30 kHz, and 30–45 kHz (Fig. 10).

To analyse the variation in peak frequency, the percentages of three peak frequency bands at different amplitudes are plotted on the right side of Fig. 10a and b. As the stress amplitude increases, the distribution of the signals shows

a similar trend. High peak frequency was not apparent in 2 stages. Lower and middle peak frequencies were the most dominant in the cyclic loading part, which means that relatively large cracks were the main part of the whole process. In contrast, the signals were lower at this stage. In addition, the AE counts also decreased in the two stages at different amplitudes. In the first and second stages, as the stress amplitude increases, the signals are characterized by relatively small-scale cracks, and the proportions of signals with frequencies are mainly in the range from 15 to 30 kHz. The 0–15 kHz signals are mainly disturbed at 10% amplitude, which leads to relatively larger cracks.

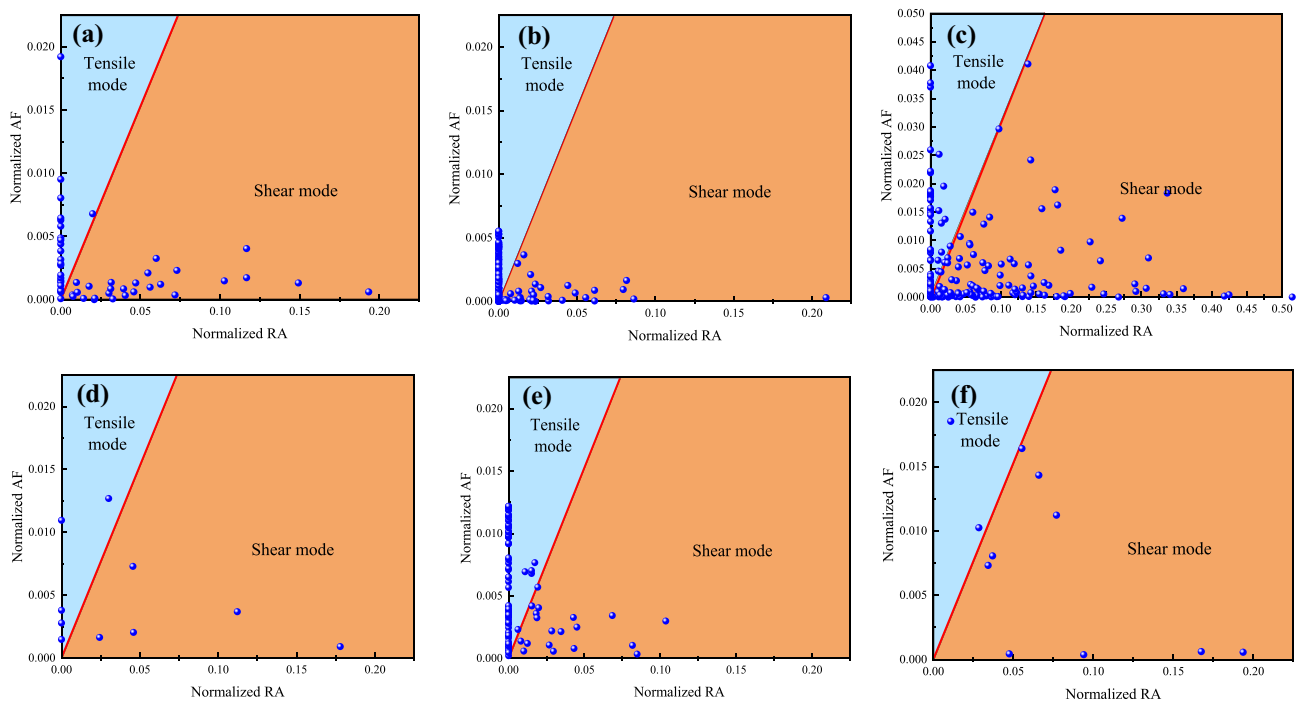


Fig. 9 Distribution of RA-AF values in sandstone at different amplitude: **a** 5% in first stage, **b** 10% in first stage, **c** 15% in first stage, **d** 5% in second stage, **e** 10% in second stage, **f** 15% in second stage

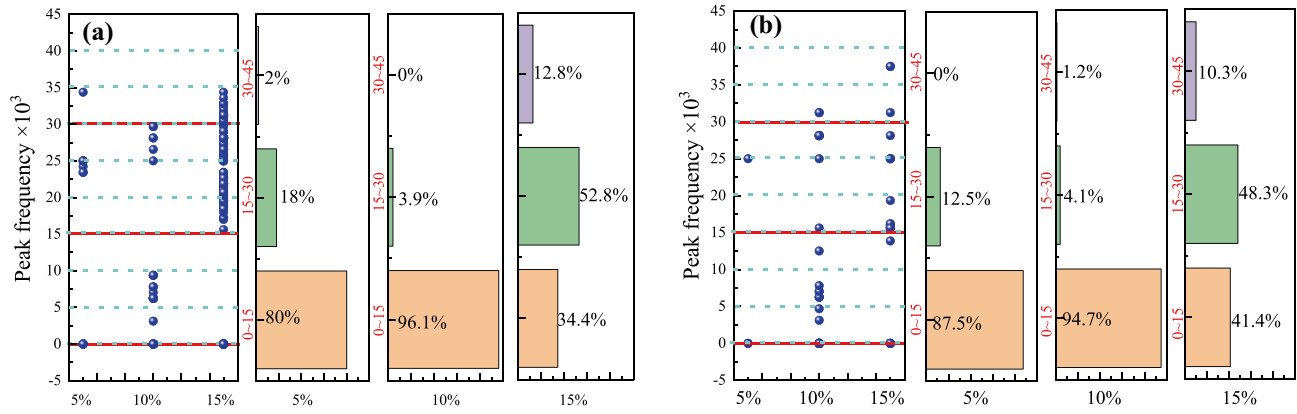


Fig. 10 Peak frequency distribution at different cyclic amplitudes. a 1st stage and b 2nd stage

Macro-failure characteristics of sandstone under a constant-cyclic test

Internal crack characteristics

Figure 11 shows an overview of the CT scanning results of three sandstone specimens under different amplitude constant-cyclic stresses. In Fig. 11b, blank regions were cracks; other regions indicated no surface cracks, demonstrating that CT scanning effectively explores the internal crack distribution in sandstone specimens.

Figure 12 demonstrates the vertical cross-section image slices and 3D fractures of the sandstone specimens under

constant-cyclic loading. When the depth \times approached 12.5 mm, relatively large cracks were observed in the cross-section under constant-cyclic compression. Furthermore, the width of the crack was larger under higher amplitude stress. The failure modes were similar to the surface fracture crack mode. When the depth \times approaches 25 mm, all cross-section cracks are located in the centre of the sandstone specimens. The crack failure mode with a lower amplitude was progradation on one side. Fault planes are more evident at 10% and 15% amplitudes. At 15% amplitude stress, both sides of the fault plane were apparent. Its failure progress was more violent compared with lower amplitude. When the depth \times approaches 37.5 mm, new cracks are initiated in the specimens under

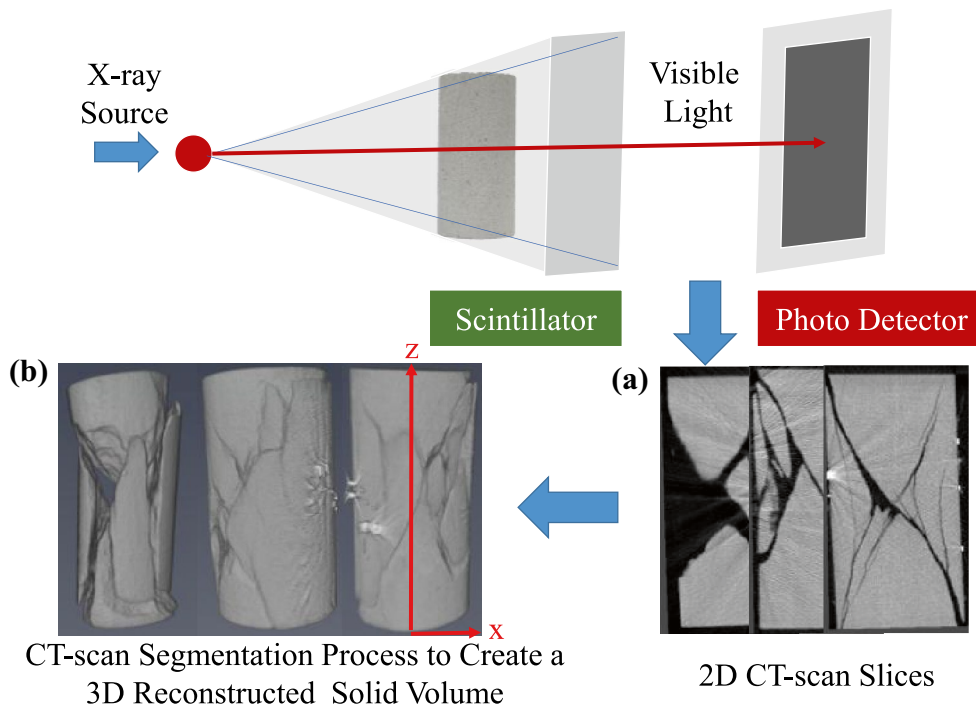


Fig. 11 Overview of the X-ray CT scanning procedure. a X-ray CT observation and b 3D reconstruction result

various amplitudes. This means that the damage degree was highly correlated with the cyclic amplitude.

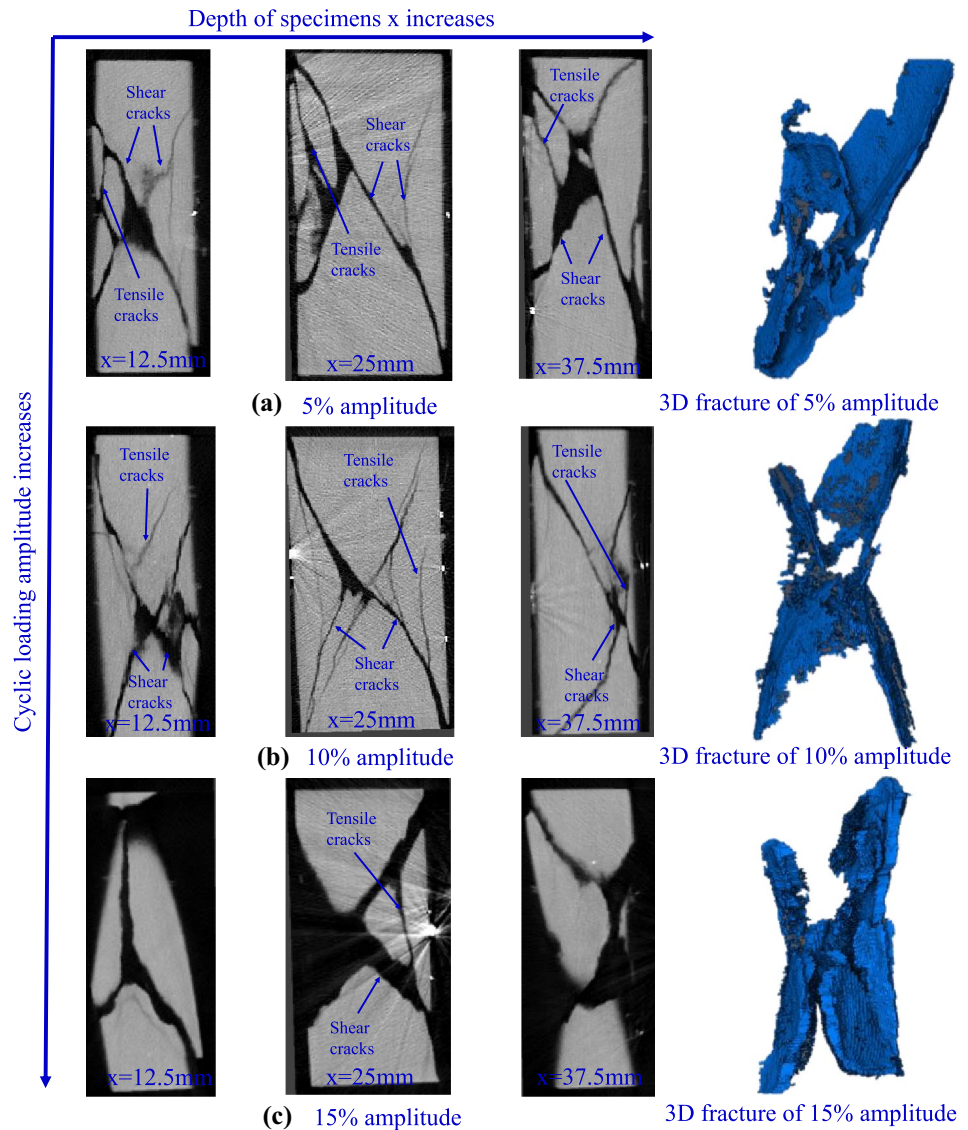
Figure 13 illustrates horizontal cross-section slices of sandstone specimens under different cyclic amplitudes. When the height z approaches 25 mm, some open cracks were observed in the slice images under various cyclic amplitudes. However, those cracks were more minor at lower amplitudes. Rock specimens can maintain their completeness. The rock specimens were shattered at higher amplitudes compared with lower cyclic amplitudes. When the height approached 50 mm, the slice images were located in the centre of the rock specimens. The number and extent of cracks were higher under higher cyclic stress amplitudes. The small and immature cracks were more noticeable than more significant degrees of crack penetration under higher cyclic amplitudes. When the height approached 75 mm, the crack distribution was similar to that at 25 mm. The crack distribution analysis of postfailure

specimens illustrates the importance of the X-ray CT scanning method to investigate the behaviour of the internal crack.

Fragmentation characteristics

The post-mortem examination of samples is helpful to obtain the fragment size distributions, rock mass distribution, and failure characteristics of sandstone specimens. Figure 14a, b, and c shows the failure characteristics and mass distribution of sandstone specimens corresponding to three typical cyclic stress amplitudes. The recovered specimens depicted the fragment size distributions, rock mass distribution, and failure patterns under different specimens. It can be observed that sandstone specimens break into blocks relatively uniformly. The fragment distribution of sandstone was not similar under different cyclic loading amplitudes. Sandstone specimens shattered into small or more significant blocks,

Fig. 12 Front vertical cross-sections and 3D fracture distribution of failed sandstone specimens under constant-cyclic stress with respect to different cyclic stress amplitudes. **a** Five percent amplitude; **b** 10% amplitude; **c** 15% amplitude



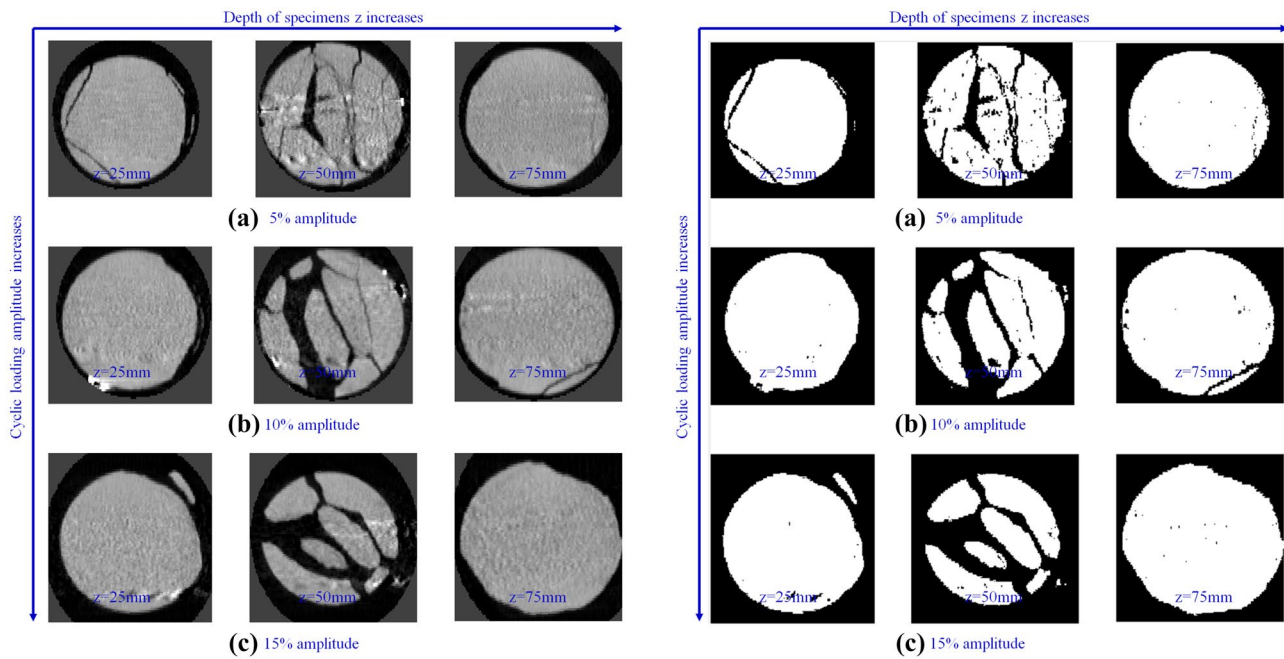


Fig. 13 Horizontal cross-section slice images of failed sandstone in the constant–cyclic test under different cyclic stress amplitudes. **a** Five per cent amplitude; **b** 10% amplitude; **c** 15% amplitude

which were more obvious under a relatively high cyclic loading amplitude. Especially when the stress amplitude reached 15%, the percentage of more significant and small blocks was higher. The sieving results of the rock mass distribution for sandstone specimens under different cyclic loading conditions are shown in Fig. 14. With the cyclic loading amplitude increasing, all sandstone specimens’ cumulative mass percentage curves show a growing percentage of small rock mass, indicating that the sandstone specimens are more polarized under a high cyclic stress amplitude. A higher cyclic loading amplitude promoted relatively more and larger cracks, which led to larger blocks. In addition, relatively small-scale blocks increased due to violent friction under higher cyclic loading amplitudes. This phenomenon can also be seen at cyclic loading amplitudes of 5% and 10%. In addition, the number of small sandstone particles increased at higher stress amplitudes. This may be due to the friction between rock particles, and a larger stress amplitude may lead to an increase in the percentage of slight sandstone particles.

Influencing mechanism of cyclic stress amplitude

In this study, the sandstone deformation under constant–cyclic tests shows a nonlinear variation with different stress amplitudes. In general, when the maximum cyclic stress is less than the cyclic threshold, the rock specimens may be strengthened by cyclic loading. Conversely, it is degraded when the

maximum cyclic stress is higher than the cyclic threshold (Günther and Salzer 2012). The influencing mechanism of the stress amplitude is illustrated in Fig. 15. The peak strength of the tested sandstone samples reaches a maximum when the loading stress is the amplitude combined with 10% UCS and constant stress. This may be due to the competition of the lower amplitude stress hardening effect and higher amplitude stress softening effect. Lower stress amplitude loading leads to rock specimen hardening, and higher amplitude loading may result in damage accumulation, leading to rock strength degradation. In addition, with increasing cyclic amplitude, the shear mode extent will increase simultaneously. A certain cyclic stress level may exist that is considered the distinction between tensile and shear modes. Overall, the stress amplitude may not be that obvious at lower stress amplitudes. With the cyclic stress levels reaching a certain level, the rock specimens experienced tensile mode initially and then approximately equal shear or tensile effect at a higher amplitude.

In addition, the larger or small-scale cracks with samples may produce resonance during the crack propagation procedure (Fig. 15a). On the one hand, this may be because the rock specimens are sensitive to specific stress amplitudes. On the other hand, this kind of frequency can also be derived from the stress waves in constant–cyclic tests. Thus, the 10% amplitude may be close to the critical amplitude that causes rock resonance and leads to relatively larger cracks dominated by resonance. However, when the stress amplitude increases, the larger cracks are mainly propagated by the stress amplitude.

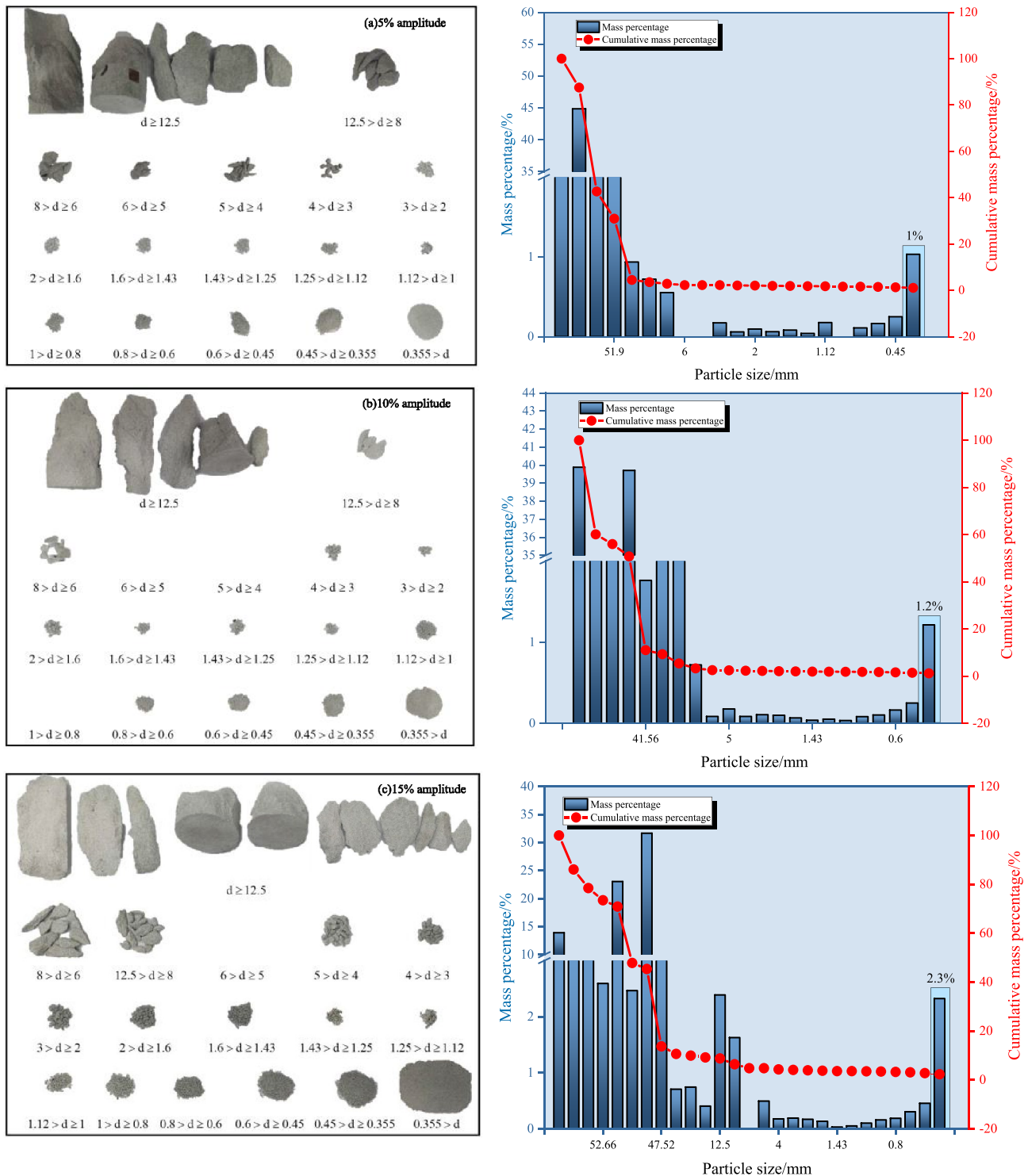


Fig. 14 Fragment size and rock mass distribution of the sandstone specimens under constant-cyclic tests, mm: **a** 5% amplitude, **b** 10% amplitude, **c** 15% amplitude

In addition, with increasing cyclic loading amplitude, all sandstone specimens' cumulative mass percentage curves show a growing percentage of small fragments, demonstrating that the sandstone specimens are more polarized in a

high cyclic stress amplitude. A higher cyclic loading amplitude promoted relatively more and larger cracks, which led to larger blocks. In addition, the percentage of small-scale blocks increased due to violent friction under higher cyclic

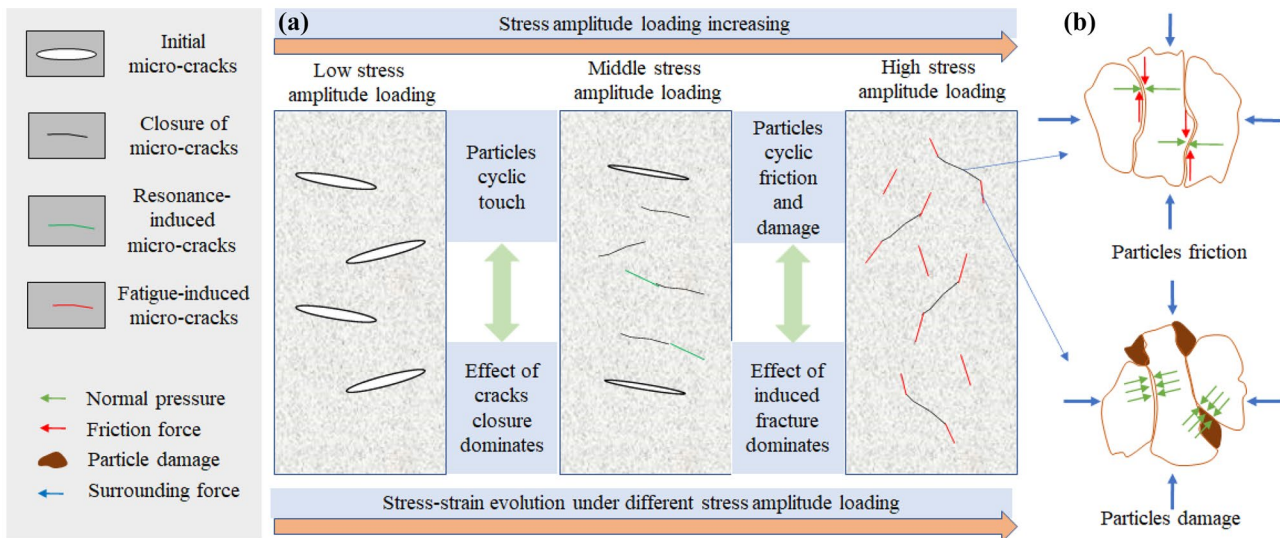


Fig. 15 The influencing mechanism of the cyclic stress amplitude on the friction force between particles of sandstone

loading amplitudes. This phenomenon can also be seen at cyclic loading amplitudes of 5% and 10%. In addition, the number of small sandstone particles increased at higher stress amplitudes. This may be due to the friction between rock particles and particle damage, and a larger stress amplitude may increase the percentage of small sandstone particles (Fig. 15b).

In underground coal mining, the overlying strata mining-induced stress boundary is under constant–cyclic loading conditions in essence. Its movement is governed by dynamic mining-induced or other kinds of disturbance with static mining-induced stress. Different disturbance effects on this boundary vary with distance and its origin properties. The actual effect on the specific boundary is different amplitude stress disturbance, which may play an essential role in this boundary movement. Our experimental results reveal that different stress amplitudes combined with constant loading may produce a hardening or softening effect. A higher stress amplitude may lead to rock failure. It is vital to avoid significant disturbances through any kind of stress relief method, such as blasting, hydraulic slotting, and fracturing. Another measure may be to maintain a proper distance from disturbance sources, especially those that quickly cause boundary movement or dynamic disasters. This may offer a reasonable explanation for why it is difficult to detect stable mining-induced boundaries.

Note that the influence of stress amplitude on sandstone is negligible because the confining stress surrounding the cylindrical surface of sandstone samples can remarkably increase the friction (Liu et al. 2021). In addition, the grain size can also affect the mechanical behaviour fracturing response. The small grain size will result in a more uniform spatial distribution of grain size (Li et al. 2018a, b).

Therefore, in the future, the confining pressure and grain size of sandstone will be studied. In addition, acoustic emission positioning techniques should be used to detect the AE source location and compare them with CT results; in this way, we can obtain more reliable results about the internal damage of sandstone.

Conclusion

This study analysed the deformation, AE, energy, and fragment evolution of sandstone under different stress amplitude constant–cyclic loadings. The real-time AE method was used during the cyclic loading stage to explore the acoustic behaviour of sandstone under uniaxial compression. The CT scanning technique also analysed the post-failure sandstone specimens under different cyclic stress amplitudes. Based on the above results, some conclusions can be obtained:

1. Based on the mechanical results of sandstone specimens under different amplitudes in constant–cyclic loading. The deformation depends strongly on the stress amplitude. As the cyclic loading amplitude increased, the strain showed a nonlinear increase, and the maximum stress showed an increase first and then decreased.
2. Elastic energy accounts for the largest proportion of all input energy. The elastic energy percentage decreases under increasing stress amplitude. The elastic energy shows an increasing trend at 5%, 10%, and 15% loading amplitudes.
3. The AE counts of sandstone under different stress amplitudes were highly dependent on the stress level. Generally, the RA-AF peak frequency distribution directly corresponds

with the stress amplitude. However, the crack propagation procedure is complex at higher stress amplitudes.

4. The internal fracture characteristics of sandstone under different stress amplitudes were investigated by slice image analysis and reconstructed 3D images of sandstone, and systematic sieving tests revealed the ultimate failure characteristics of the sandstone. Shear failure patterns are the main part of the post-specimens. The failure modes in the CT scanning slice image varied with the depth and height position. With the increase in the stress amplitude, the percentage of large block and slight block mass increase, which means the uniformity of rock failure increases.

Author contribution All authors contributed to the study conception and design. Material preparation, data collection, and analysis were performed by Bichuan Zhang, Yunpei Liang, Zhanyi Zhao, Quanle Zou, Haolong Zheng, Yanhao Ning, Fanjie Kong, and Qican Ran. The first draft of the manuscript was written by Bichuan Zhang, and all authors commented on previous versions of the manuscript. All authors read and approved the final manuscript. Conceptualization: Bichuan Zhang; methodology: Quanle Zou; formal analysis and investigation: Haolong Zheng, Qican Ran, and Yanhao Ning; writing, original draft preparation: Bichuan Zhang; writing, review and editing: Bichuan Zhang, Zhanyi Zhao, and Fanjie Kong; funding acquisition: Yunpei Liang and Quanle Zou; resources: Quanle Zou; and supervision: Yunpei Liang.

Funding This study was financially supported by the National Key R&D Program of China (Grant No. 2022YFC3004704), the National Natural Science Foundation of China (52174166 and 52074041), the “Overall Rationing System” Project of Chongqing Talent Program (cstc2022ycjh-bgzxm0077), the Fundamental Research Funds for the Central Universities (2020CDJ-LHZZ-002), and the Natural Science Foundation of Chongqing, China (cstc2020jcyj-msxmX0836), which are gratefully acknowledged.

Data Availability All data, models, and codes generated or used during the study are available from the corresponding author upon request.

Declarations

Conflict of interest The authors declare no competing interests.

References

- Akesson U, Hansson J, Stigh J (2004) Characterisation of microcracks in the Bohus granite, western Sweden, caused by uniaxial cyclic loading. *Eng Geol* 72:131–142. <https://doi.org/10.1016/j.enggeo.2003.07.001>
- Ammirati L, Di Martire D, Bordicchia F, Calcaterra D, Russo G, Mondillo N (2022) Semi-real time systems for subsidence monitoring in areas affected by underground mining: the example of the Nuraxi-Figus coal district (Sardinia, Italy). *Int J Coal Sci Technol* 9:1–15. <https://doi.org/10.1007/s40789-022-00559-0>
- Bagde MN, Petros V (2009) Fatigue and dynamic energy behaviour of rock subjected to cyclical loading. *Int J Rock Mech Min Sci* 46:200–209. <https://doi.org/10.1016/j.ijrmm.2008.05.002>
- Cai YD, Liu DM, Mathews JP, Pan ZJ, Elsworth D, Yao YB, Li JQ, Guo XQ (2014) Permeability evolution in fractured coal - combining triaxial confinement with X-ray computed tomography, acoustic emission and ultrasonic techniques. *Int J Coal Geol* 122:91–104. <https://doi.org/10.1016/j.coal.2013.12.012>
- Cerfontaine B, Collin F (2018) Cyclic and fatigue behaviour of rock materials: review, interpretation and research perspectives. *Rock Mech* 51:391–414. <https://doi.org/10.1007/s00603-017-1337-5>
- Demirel N (2011) Effects of the rock mass parameters on the dragline excavation performance. *J Min Sci* 47:441–449. <https://doi.org/10.1134/S106273914704006x>
- Deng HF, Hu Y, Li JL, Wang Z, Zhang XJ, Zhang HB (2017) Effects of frequency and amplitude of cyclic loading on the dynamic characteristics of sandstone. *Soils Rocks* 38:3402–3415. <https://doi.org/10.16285/j.rsm.2017.12.002>
- Dong L, Tao Q, Hu Q, Deng S, Chen Y, Luo Q, Zhang X (2022) Acoustic emission source location method and experimental verification for structures containing unknown empty areas. *Int J Min Sci Technol*. <https://doi.org/10.1016/j.mtcomm.2022.104582>
- Du H, Song DQ, Chen Z, Guo ZZ (2020) Experimental study of the influence of structural planes on the mechanical properties of sandstone specimens under cyclic dynamic disturbance. *Energy Sci Eng* 8:4043–4063. <https://doi.org/10.1002/ese3.794>
- Du K, Sun Y, Zhou J, Wang S-f, Tao M, Yang C, Khandelwal M (2021) Low amplitude fatigue performance of sandstone, marble, and granite under high static stress. *Geomech. Geophys. Geo-Energy Geo-Resour* 7:1–21. <https://doi.org/10.1007/s40948-021-00266-1>
- Duan HQ, Yang YJ (2018) Deformation and dissipated energy of sandstone under uniaxial cyclic loading. *Geotech Geol Eng* 36:611–619. <https://doi.org/10.1007/s10706-017-0306-9>
- Erarslan N (2016) Microstructural investigation of subcritical crack propagation and fracture process zone (FPZ) by the reduction of rock fracture toughness under cyclic loading. *Eng Geol* 208:181–190. <https://doi.org/10.1016/j.enggeo.2016.04.035>
- Fuenkajorn K, Phueakphum D (2010) Effects of cyclic loading on mechanical properties of Maha Sarakham salt. *Eng Geol* 112:43–52. <https://doi.org/10.1016/j.enggeo.2010.01.002>
- Günther R, Salzer K (2012). Advanced strain-hardening approach. *Mechanical Behaviour of Salt VII*: 13–22.
- He MM, Li N, Chen YS, Zhu CH (2015) An experimental study of dynamic behaviors of rock under stepwise cyclic loading. *Soils Rocks* 36:2907–2913. <https://doi.org/10.16285/j.rsm.2015.10.021>
- He S, Qin M, Qiu L, Song D, Zhang X (2022) Early warning of coal dynamic disaster by precursor of AE and EMR “quiet period”. *Int J Coal Sci Technol* 9:1–14. <https://doi.org/10.1007/s40789-022-00514-z>
- Hua AZ, You MQ (2001) Rock failure due to energy release during unloading and application to underground rock burst control. *Tunn Undergr Space Technol* 16:241–246. [https://doi.org/10.1016/S0886-7798\(01\)00046-3](https://doi.org/10.1016/S0886-7798(01)00046-3)
- K M (1962) Study of the elastic shocks caused by the fracture of heterogeneous materials and its relation to earthquake phenomena. *Bull Earthq Res Inst* 40:125–173
- Kao CS, Carvalho FCS, Labuz JF (2011) Micromechanisms of fracture from acoustic emission. *Int J Rock Mech Min Sci* 48:666–673. <https://doi.org/10.1016/j.ijrmm.2011.04.001>
- Khandelwal M, Singh TN (2009) Prediction of blast-induced ground vibration using artificial neural network. *Int J Rock Mech Min Sci* 46:1214–1222. <https://doi.org/10.1016/j.ijrmm.2009.03.004>
- Konicek P, Soucek K, Stas L, Singh R (2013) Long-hole destress blasting for rockburst control during deep underground coal mining. *Int J Rock Mech Min Sci* 61:141–153. <https://doi.org/10.1016/j.ijrmm.2013.02.001>
- Lavrov A (2001) Kaiser effect observation in brittle rock cyclically loaded with different loading rates. *Mech Mater* 33:669–677. [https://doi.org/10.1016/s0167-6636\(01\)00081-3](https://doi.org/10.1016/s0167-6636(01)00081-3)
- Li Q, Li J, Duan L, Tan S (2021) Prediction of rock abrasivity and hardness from mineral composition. *Int J Rock Mech Min Sci* 140:104658. <https://doi.org/10.1016/j.ijrmm.2021.104658>

- Li T, Pei X, Guo J, Meng M, Huang R (2020) An energy-based fatigue damage model for sandstone subjected to cyclic loading. *Rock Mech* p. 5069–5079. <https://doi.org/10.1007/s00603-020-02209-w>
- Li X, Gong F, Tao M, Dong L, Du K, Ma C, Zhou Z, Yin T (2017) Failure mechanism and coupled static-dynamic loading theory in deep hard rock mining: a review. *J Rock Mech Geotech Eng* 9:767–782. <https://doi.org/10.1016/j.jrmge.2017.04.004>
- Li XF, Li X, Li HB, Zhang QB, Zhao J (2018a) Dynamic tensile behaviours of heterogeneous rocks: the grain scale fracturing characteristics on strength and fragmentation. *Int J Impact Eng* 118:98–118. <https://doi.org/10.1016/j.ijimpeng.2018.04.006>
- Li Y, Zhang S, Zhang X (2018b) Classification and fractal characteristics of coal rock fragments under uniaxial cyclic loading conditions. *Arab J Geosci* 11. <https://doi.org/10.1007/s12517-018-3534-2>
- Liang Y, Ran Q, Zou Q, Zhang B, Hong Y (2022) Experimental study of mechanical behaviors and failure characteristics of coal under true triaxial cyclic loading and unloading and stress rotation. *Nat Resour J* 31: 971–991. <https://doi.org/10.1007/s11053-022-10022-1>
- Liu X, Liu Z, Li X, Gong F, Du K (2020) Experimental study on the effect of strain rate on rock acoustic emission characteristics. *Int J Rock Mech Min Sci* 133:104420. <https://doi.org/10.1016/j.ijrmm.2020.104420>
- Liu Y, Dai F, Dong L, Xu NW, Feng P (2018) Experimental investigation on the fatigue mechanical properties of intermittently jointed rock models under cyclic uniaxial compression with different loading parameters. *Rock Mech* 51:47–68. <https://doi.org/10.1007/s00603-017-1327-7>
- Liu Y, Dai F, Fan PX, Xu NW, Dong L (2017) Experimental investigation of the influence of joint geometric configurations on the mechanical properties of intermittently jointed rock models under cyclic uniaxial compression. *Rock Mech* 50:1453–1471. <https://doi.org/10.1007/s00603-017-1190-6>
- Liu Y, Huang D, Cen D, Zhong Z, Gong F, Wu Z, Yang Y (2021) Tensile strength and fracture surface morphology of granite under confined direct tension test. *Rock Mech* 54:4755–4769. <https://doi.org/10.1007/s00603-021-02543-7>
- Lockner D (1993) The role of acoustic-emission in the study of rock fracture. *Int J Rock Mech Min Sci* 30:883–899. [https://doi.org/10.1016/0148-9062\(93\)90041-b](https://doi.org/10.1016/0148-9062(93)90041-b)
- Luo D, Su G, Zhang G (2019) True-triaxial experimental study on mechanical behaviours and acoustic emission characteristics of dynamically induced rock failure. *Rock Mech* 53:1205–1223. <https://doi.org/10.1007/s00603-019-01970-x>
- Meng Q, Zhang M, Han L, Pu H, Chen Y (2018) Acoustic emission characteristics of red sandstone specimens under uniaxial cyclic loading and unloading compression. *Rock Mech* 51:969–988. <https://doi.org/10.1007/s00603-017-1389-6>
- Meng Q, Zhang M, Zhang Z, Han L, Pu H (2019) Research on non-linear characteristics of rock energy evolution under uniaxial cyclic loading and unloading conditions. *Environ Earth Sci* 78:1–20. <https://doi.org/10.1007/s12665-019-8638-9>
- Momeni A, Karakus M, Khanlari GR, Heidari M (2015) Effects of cyclic loading on the mechanical properties of a granite. *Int J Rock Mech Min Sci* 100:89–96. <https://doi.org/10.1016/j.ijrmm.2015.03.029>
- Munoz H, Taheri A (2017) Local damage and progressive localization in porous sandstone during cyclic loading. *Rock Mech* 50:3253–3259. <https://doi.org/10.1007/s00603-017-1298-8>
- Ning S, Yang YJ, Lv JK, Duan HQ (2019) The fractal characteristics of coal sample's fragments subjected to cyclic loading. *Geotech Geol Eng* 37:2267–2281. <https://doi.org/10.1007/s10706-018-0735-0>
- Ran QC, Liang YP, Zou QL, Hong Y, Zhang BC, Liu H, Kong FJ (2023) Experimental investigation on mechanical characteristics of red sandstone under graded cyclic loading and its inspirations for stability of overlying strata. *Geomech Geophys Geo-Energy Geo-Resour* 9:11–23. <https://doi.org/10.1007/s40948-023-00555-x>
- Rodriguez P, Celestino TB (2019) Application of acoustic emission monitoring and signal analysis to the qualitative and quantitative characterization of the fracturing process in rocks. *Eng Fract Mech* 210: 54–69. <https://doi.org/10.1016/j.engfracmech.2018.06.027>
- Ruck M, Rahner R, Sone H, Dresen G (2017) Initiation and propagation of mixed mode fractures in granite and sandstone. *Tectonophysics* 717:270–283. <https://doi.org/10.1016/j.tecto.2017.08.004>
- Sagar RV, Prasad BKR (2012) A review of recent developments in parametric based acoustic emission techniques applied to concrete structures. *Nondestructive Testing and Evaluation* 27:47–68. <https://doi.org/10.1080/10589759.2011.589029>
- Sang GJ, Liu SM, Elsworth D (2020) Quantifying fatigue-damage and failure-precursors using ultrasonic coda wave interferometry. *Int J Rock Mech Min Sci* 131:104366. <https://doi.org/10.1016/j.ijrmm.2020.104366>
- Shi CH, Ding ZD, Lei MF, Peng LM (2014) Accumulated deformation behavior and computational model of water-rich mudstone under cyclic loading. *Rock Mech* 47:1485–1491. <https://doi.org/10.1007/s00603-013-0427-2>
- Shirani Faradonbeh R, Taheri A, Karakus M (2021) failure behaviour of a sandstone subjected to the systematic cyclic loading: insights from the double-criteria damage-controlled test method. *Rock Mech* 54:5555–5575. <https://doi.org/10.1007/s00603-021-02553-5>
- Sun Y, Zuo J, Karakus M, Wang J (2019) Investigation of movement and damage of integral overburden during shallow coal seam mining. *Int J Rock Mech Min Sci* 117:63–75. <https://doi.org/10.1016/j.ijrmm.2019.03.019>
- Taheri A, Royle A, Yang Z, Zhao Y (2016) Study on variations of peak strength of a sandstone during cyclic loading. *Geomech Geophys Geo-Energy Geo-Resour* 2:1–10. <https://doi.org/10.1007/s40948-015-0017-8>
- Vaneghi RG, Ferdosi B, Okoth AD, Kuek B (2018) Strength degradation of sandstone and granodiorite under uniaxial cyclic loading. *J Rock Mech Geotech Eng* 10:117–126. <https://doi.org/10.1016/j.jrmge.2017.09.005>
- Vaneghi RG, Thoeni K, Dyskin AV, Sharifzadeh M, Sarmadivaleh M (2020) Strength and damage response of sandstone and granodiorite under different loading conditions of multistage uniaxial cyclic compression. *Int J Geomech* 20:04020159. [https://doi.org/10.1061/\(ASCE\)GM.1943-5622.0001801](https://doi.org/10.1061/(ASCE)GM.1943-5622.0001801)
- Wang G, Guo K, Christianson M, Konietzky H (2011) Deformation characteristics of rock salt with mudstone interbeds surrounding gas and oil storage cavern. *Int J Rock Mech Min Sci* 48:871–877. <https://doi.org/10.1016/j.ijrmm.2011.06.012>
- Wang Y, Hou ZQ, Hu YZ (2019) In situ X-ray computed tomography experiment on mesodamage evolution of subgrade bimsolil during cycle loading. *J Mater Civ Eng* 31. [https://doi.org/10.1061/\(ASCE\)Mt.1943-5533.0002796](https://doi.org/10.1061/(ASCE)Mt.1943-5533.0002796)
- Wang Y, Hu Y, Gao S (2021) Dynamic mechanical behaviors of interbedded marble subjected to multi-level uniaxial compressive cyclic loading conditions: an insight into fracture evolution analysis. *Eng Fract Mech* 241:107410. <https://doi.org/10.1016/j.engfracmech.2020.107410>
- Wang Y, Li CH, Han JQ (2020) On the effect of stress amplitude on fracture and energy evolution of pre-flawed granite under uniaxial increasing-amplitude fatigue loads. *Eng Fract Mech* 240:107366. <https://doi.org/10.1016/j.engfracmech.2020.107366>
- Xia Z, Yao Q, Meng G, Xu Q, Tang C, Zhu L, Wang W, Shen Q (2021) Numerical study of stability of mining roadways with 6.0-m section coal pillars under influence of repeated mining. *Int J Rock Mech Min Sci* 138:104–112. <https://doi.org/10.1016/j.ijrmm.2021.104641>

- Xiao F, Jiang D, Wu F, Zou Q, Chen J, Chen B, Sun Z (2020) Effects of prior cyclic loading damage on failure characteristics of sandstone under true-triaxial unloading conditions. *Int J Rock Mech Min Sci* 132:104379. <https://doi.org/10.1016/j.ijrmms.2020.104379>
- Yang J, Dai J, Yao C, Jiang S, Zhou C, Jiang Q (2020a) Estimation of rock mass properties in excavation damage zones of rock slopes based on the Hoek-Brown criterion and acoustic testing. *Int J Rock Mech Min Sci* 126:104192. <https://doi.org/10.1016/j.ijrmms.2019.104192>
- Yang S-Q, Hu B (2018) Creep and long-term permeability of a red sandstone subjected to cyclic loading after thermal treatments. *Rock Mech* 51:2981–3004. <https://doi.org/10.1007/s00603-018-1528-8>
- Yang S-Q, Huang Y-H, Tang J-Z (2020b) Mechanical, acoustic, and fracture behaviors of yellow sandstone specimens under triaxial monotonic and cyclic loading. *Int J Rock Mech Min Sci* 130:104268. <https://doi.org/10.1016/j.ijrmms.2020.104268>
- Yang XB, Han XX, Liu EL, Zhang ZP, Wang XY (2018) Experimental study on the acoustic emission characteristics of non-uniform deformation evolution of granite under cyclic loading and unloading test. *Soils Rocks* 39:2732–2739. <https://doi.org/10.16285/j.rsm.2018.0048>
- Young RP, Nasser MHB, Sehzadeh M (2020) Mechanical and seismic anisotropy of rocks from the ONKALO underground rock characterization facility. *Int J Rock Mech Min Sci* 126:104190. <https://doi.org/10.1016/j.ijrmms.2019.104190>
- Zhang JZ, Zhou XP (2020) Forecasting catastrophic rupture in brittle rocks using precursory AE time series. *J Geophys Res Solid Earth* 125. <https://doi.org/10.1029/2019jb019276>
- Zhang JZ, Zhou XP (2022) Fracture process zone (FPZ) in quasi-brittle materials: review and new insights from flawed granite subjected to uniaxial stress. *Eng Fract Mech* 274. <https://doi.org/10.1016/j.engfracmech.2022.108795>
- Zhang JZ, Zhou XP, Du YH Cracking behaviors and acoustic emission characteristics in brittle failure of flawed sandstone: a true triaxial experiment investigation. *Rock Mech*. <https://doi.org/10.1007/s00603-022-03087-0>
- Zhang Q, Wang E, Feng X, Wang C, Qiu L, Wang H (2021) Assessment of rockburst risk in deep mining: an improved comprehensive index method. *Nat Resour J* 30:1817–1834. <https://doi.org/10.1007/s11053-020-09795-0>
- Zhang T, Yu L, Su H, Zhang Q, Chai S (2022) Experimental and numerical investigations on the tensile mechanical behavior of marbles containing dynamic damage. *Int J Min Sci Technol* 32:89–102. <https://doi.org/10.1016/j.ijmst.2021.08.002>
- Zhang X, Pak RYS, Gao Y, Liu C, Zhang C, Yang J, He M (2020) Field experiment on directional roof presplitting for pressure relief of retained roadways. *Int J Rock Mech Min Sci* 134:104436. <https://doi.org/10.1016/j.ijrmms.2020.104436>
- Zhang Y, Feng X-T, Yang C, Zhang X, Sharifzadeh M, Wang Z (2019) Fracturing evolution analysis of Beishan granite under true triaxial compression based on acoustic emission and strain energy. *Int J Rock Mech Min Sci* 117:150–161. <https://doi.org/10.1016/j.ijrmms.2019.03.029>
- Zhang ZT, Zhang R, Xie HP, Gao MZ, Xie J (2016) Mining-induced coal permeability change under different mining layouts. *Rock Mech* 49:3753–3768. <https://doi.org/10.1007/s00603-016-0979-z>
- Zhao, Zhang LY, Wang WJ, Wan W, Li SQ, Ma WH, Wang YX (2017) Creep behavior of intact and cracked limestone under multi-level loading and unloading cycles. *Rock Mech* 50:1409–1424. <https://doi.org/10.1007/s00603-017-1187-1>
- Zhao K, Ma H, Yang C, Chen X, Liu Y, Liang X, Cai R (2021) Damage evolution and deformation of rock salt under creep-fatigue loading. *Rock Mech* 1985–1997. <https://doi.org/10.1007/s00603-020-02342-6>
- Zhou HW, Wang ZH, Wang CS, Liu JF (2019) On acoustic emission and post-peak energy evolution in Beishan granite under cyclic loading. *Rock Mech* 52:283–288. <https://doi.org/10.1007/s00603-018-1614-y>
- Zhu W, Li S, Li S, Niu L (2019) Influence of dynamic disturbance on the creep of sandstone: an experimental study. *Rock Mech* 52:1023–1039. <https://doi.org/10.1007/s00603-018-1642-7>
- Zhu X-Y, Chen X-D, Dai F (2020) Mechanical properties and acoustic emission characteristics of the bedrock of a hydropower station under cyclic triaxial loading. *Rock Mech* 53:5203–5221. <https://doi.org/10.1007/s00603-020-02218-9>
- Zou Q, Chen Z, Cheng Z, Liang Y, Xu W, Wen P, Zhang B, Liu H, Kong F (2022a) Evaluation and intelligent deployment of coal and coalbed methane coupling coordinated exploitation based on Bayesian network and cuckoo search. *Int J Min Sci Technol*. <https://doi.org/10.1016/j.ijmst.2022.11.002>
- Zou Q, Zhou X, Wang R, Ning Y, Chen Z, Kong F, Liu Y (2022b) Load-carrying and energy-absorbing performance of honeycombs with different cross sections under cyclic loading. *Mater. Today Commun* 33:104582. <https://doi.org/10.1016/j.mtcomm.2022.104582>

Springer Nature or its licensor (e.g. a society or other partner) holds exclusive rights to this article under a publishing agreement with the author(s) or other rightsholder(s); author self-archiving of the accepted manuscript version of this article is solely governed by the terms of such publishing agreement and applicable law.